

# Numerical Investigation of two 3-D Designed Profiles in a 2-Stage Turbine with Shrouded Bladings

Dieter E. BOHN<sup>1</sup>, Ingo BALKOWSKI<sup>1</sup>, Christian TÜMMERS<sup>1</sup> and Michael SELL<sup>2</sup>

<sup>1</sup>Institute of Steam and Gas Turbines, Aachen University  
D-52056 Aachen, Germany

Phone: +49-241-80-25451. FAX: +49-241-80-22307, E-mail: post-bohn@idg.rwth-aachen.de

<sup>2</sup>ALSTOM Power, 5401 Baden, Switzerland

## ABSTRACT

An important goal in the development of turbine bladings is to improve their efficiency for an optimized usage of energy resources. This requires a detailed insight into the complex 3D-flow phenomena in multi-stage turbines. In order to investigate the flow characteristics of modern highly loaded turbine profiles a test rig with a two stage axial turbine has been set up at the Institute of Steam and Gas Turbines, Aachen University. The test rig is especially designed to investigate different blading designs.

In order to analyze the influence of the blade design on the secondary flow and to discuss the effects of the blade loading, the 3D flow through the 2-stage turbine is investigated numerically, using the steady Navier-Stokes inhouse computer code, CHT-Flow. The simulations include a comparison of two bow-designed blades with different design criteria. Blading A is designed to minimize the secondary flow phenomena near the endwalls in order to achieve a homogenous mass flow throughout the passage height. This blade design will be compared to a blading with an alternate design philosophy, especially developed for this test turbine (blading B). This blading concentrates the flow in the middle of the passage in order to keep the main flow away from the secondary flow regions at the endwalls of the blade. The investigations will be done with focus on the secondary flow phenomena in the second guide vane. For a detailed analysis of the blade load the design point and an off-design point are simulated for each blading. The results show a higher efficiency for blading A.

The flow conditions are taken from experimental investigations performed at the Institute of Steam and Gas Turbines, Aachen University. In the experimental setup, the turbine is operated at a low pressure ratio of 1.4 with an inlet pressure of  $3.2 \cdot 10^5$  Pa. The numerical results will also be compared to the corresponding experimental data at the outlet of the second stage.

## NOMENCLATURE

D	[ mm ]	diameter
h	[ mm ]	passage height coordinate
H	[ mm ]	passage height
L	[ mm ]	vane height
n	[ rpm ]	rotating speed
p	[ Pa ]	pressure

Copyright © 2003 by GTSJ

Manuscript Received on March 31, 2003

$\Delta x$	[ mm ]	axial distance
X	[ mm ]	axial chord length of the blade
$\alpha$	[ deg ]	swirl angle
$\beta$	[ deg ]	pitch angle
$\varphi$	[ deg ]	circumferential coordinate
$\pi$	[ - ]	pressure ratio
$\xi, \eta, \zeta$	[ mm ]	arbitrary coordinates
PS		pressure side
SS		suction side
MP10		measurement plane upstream of the first stage
MP22		measurement plane downstream of the second stage

*Subscripts*

t	total
10	at measurement plane MP10
22	at measurement plane MP22

## INTRODUCTION

Improving the efficiency of a turbine stage can be done in several ways, like endwall contouring or a 3-D blade design. Both methods influence mainly the secondary flows at the hub and the casing of the blade. By endwall contouring, the radial pressure field is influenced in such a way, that tip clearance flows and passage vortices are minimized. This leads to an increased efficiency of the turbine (Bohn et al. 2002). The 3-D blade design also influences the radial pressure field. Here the secondary flow loss mechanisms like the passage or the horseshoe-vortex are reduced by a bow design of the blade (Van den Braembussche et al. 2001).

A detailed survey over secondary flow models is given by Sieverding (1984) and Hirsch (1994). The experimental work of Sieverding and Van den Bosch (1983), Marchal and Sieverding (1977) and Moore and Smith (1983) have contributed to develop and refine these models. Understanding of the basic mechanisms relating development and propagation of secondary flow phenomena is a key to reduce aerodynamic losses.

The analysis of these complex flow phenomena by CFD necessitates the use of 3D Navier-Stokes solvers. With these methods Zimmermann (1992) has worked out the losses influenced by the secondary flows. Bassi and Savini (1992) and Nikolaou et al (1997) examined the vortices in the blade channel. Further experimental and numerical investigations in the field of secondary flow phenomena in multistage turbines were completed by Bohn et. al. (1997, 2000, 2003).

The secondary flow phenomena are also mainly influenced by the blade geometry and the blade load. In order to capture these effects a detailed analysis of the flow through a two-stage turbine is simulated numerically, comparing two different blade designs. For both configurations a design point and an off-design point will be simulated numerically.

## INVESTIGATED CONFIGURATION

### Test Turbine Set Up

The investigated two-stage test turbine with shrouded bladings has been built up at the Institute of Steam and Gas Turbines, Aachen University. Figure 1 shows the meridional cross-section of the air turbine. It is supplied with air from compressors at a maximum inlet pressure of  $3.2 \cdot 10^5$  Pa with a mass flow of maximum 7.4 kg/s. The air is pumped in a closed cycle. The temperature at the compressor and turbine inlets are adjusted by two water driven air coolers. The pressure level in the closed cycle is adjusted by a compression load supply and an exhaust valve. The power of the rotor is dissipated in a water break mounted in a momentum pendulum with hydrostatic bearings. Via these components, the momentum of the rotor can be measured very sensitively. The stator blades are fixed in an inner casing. In order to perform changes of the configuration the turbine is constructed in a modular way. The design of the turbine is chosen in such a way that a different rotor and guide blade carrier can be built in easily.

The radial sealing gap between blade shroud and housing as well as vane shroud and rotor shaft are adjusted to "zero" by use of ground seals. Therefore, the rotating speed is increased very slowly after warming up the machine to operating temperature. During this process the steel rotor shrouds and the steel sealing rings are grinding into the soft coatings inside the housing and on the guide vane shrouds. Measurements during operation using electrographic pens proved radial gaps lower than the measurement accuracy of 0.03mm. Thus, the leakage flow can be avoided nearly completely.

The geometrical data of the turbine and the operating conditions during the investigations are listed in Table 1. The operating conditions are the same for both bladings. Operating point 1 (OP1) is the design point and OP2 is the off-design point of the turbine.

### Investigated Bladings

Blading A is designed to realize a radially homogenous flow across the passage. This is achieved by a widening of the flow channel near the tip and the hub, reducing the secondary flow phenomena near the endwalls.

Due to the design of blading B, which was especially developed for this test turbine, the main flow is drawn to the middle of the passage height, in order to maintain the main flow in the region of best aerodynamic performance. Here, the increase of secondary flow regions at the tip and the hub are deliberately accepted.

Table 1 Test conditions

Average diameter, MP10	$D_{a,10}$	[mm]	410.5
Average diameter, MP22	$D_{a,22}$	[mm]	434.5
Vane height, stator 1st stage	$L_1$	[mm]	60.5
Blade height, rotor, 2nd stage	$L_2$	[mm]	74.5
Rotor blades / stator vanes	$z$	[ $-$ ]	48 / 48
Design criterium blading A	homogenous flow throughout passage		
Design criterium blading B	flow concentrated in middle of passage		
Inlet pressure	$p_t$	[ $\cdot 10^5$ Pa <sub>abs</sub> ]	3.2
Pressure ratio OP1; OP2	$\pi$	[ $-$ ]	1.4; 1.4
Rotating speed OP1; OP2	$n$	[rpm]	4763; 3780

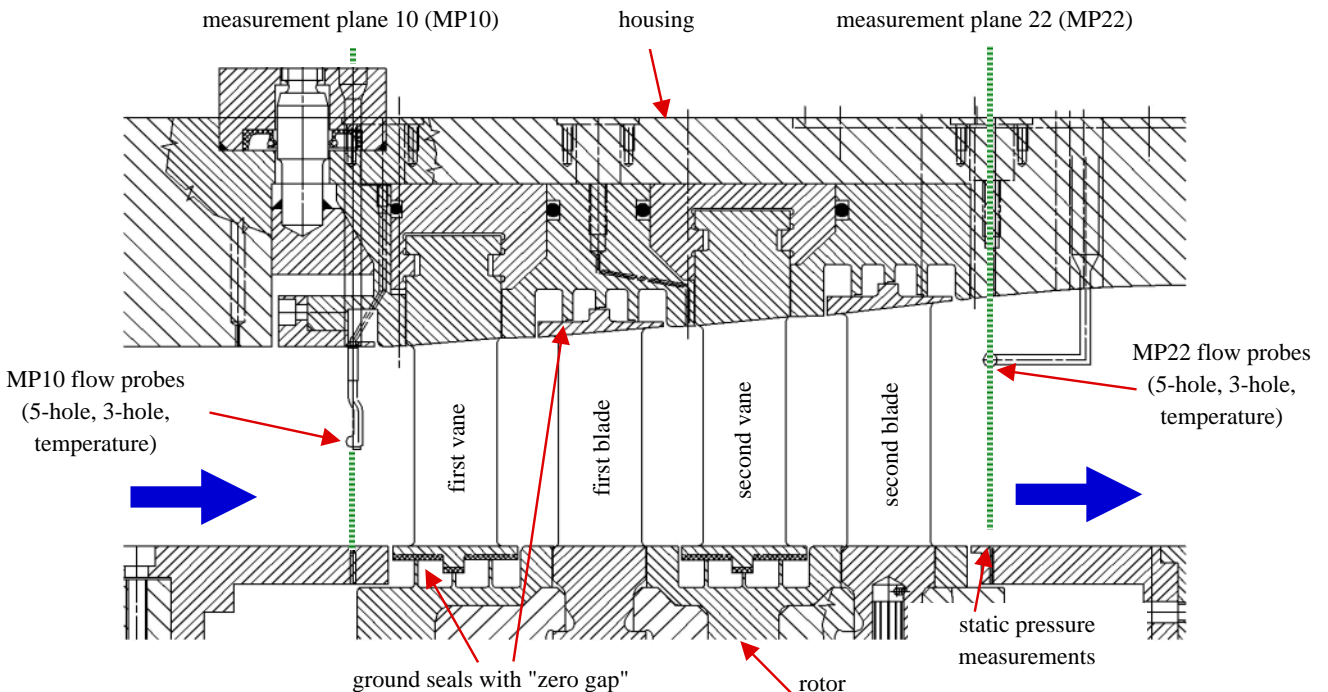


Fig. 1 Test turbine

## NUMERICAL METHOD AND GRID

The numerical scheme for the simulation of the fluid flow works on the basis of an implicit finite volume method combined with a multi-block technique for structured grids. The physical domain is divided into separate blocks, and the full, compressible, three-dimensional Navier-Stokes equations are solved in the fluid blocks. The governing equations for the conservative variables in arbitrary, body-fitted coordinates  $\xi, \eta, \zeta$  with the fluxes in normal directions to the cell faces, for which  $\xi, \eta, \zeta$  are constant, read for the fluid flow:

$$\mathbf{U}_t + \mathbf{E}_\xi + \mathbf{F}_\eta + \mathbf{G}_\zeta = \mathbf{0} \quad (1)$$

with:

$$\mathbf{U} = J \cdot (\rho, \rho u, \rho v, \rho w, \rho e_t)^T \quad (2)$$

$$\mathbf{E} = J \cdot (\mathbf{E} \cdot \xi_x + \mathbf{F} \cdot \xi_y + \mathbf{G} \cdot \xi_z) \quad (3)$$

$$\mathbf{E} = \begin{pmatrix} \rho u \\ \rho u^2 - \tau_{xx} \\ \rho uv - \tau_{xy} \\ \rho uw - \tau_{xz} \\ (\rho e - \tau_{xx})u - \tau_{xy}v - \tau_{xz}w + q_x \end{pmatrix} \quad (4)$$

The fluxes  $\mathbf{F}$  and  $\mathbf{G}$  are obtained analogously.  $\mathbf{U}$  is the vector of the conservative variables,  $\tau_{xx}, \dots$  etc. are the components of the Reynolds stress tensor,  $\mathbf{q}$  is the heat flux vector.  $J$  is the cell volume and the expressions  $\xi_x, \dots$  are the metrics, which result

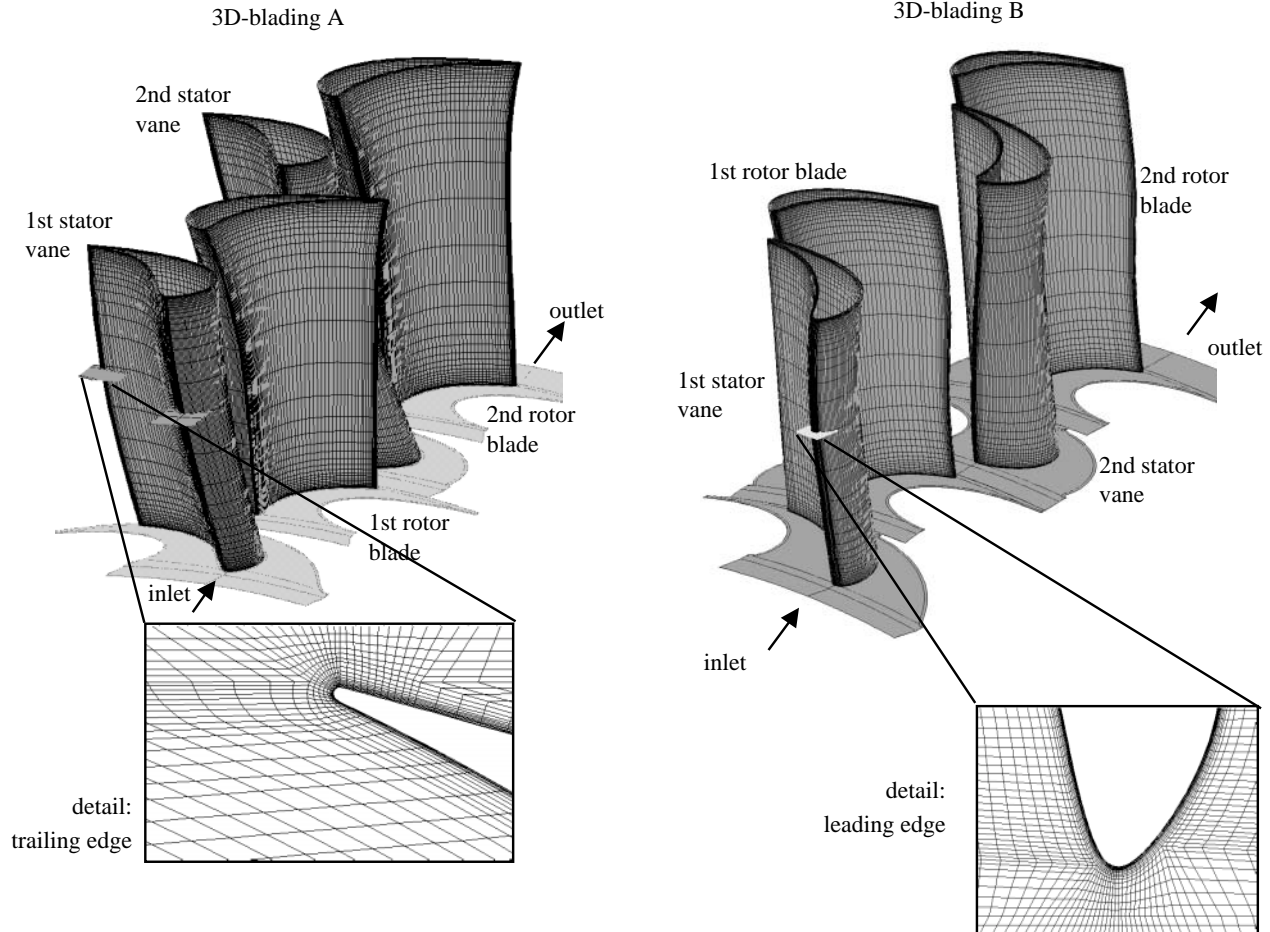


Fig. 2 Structured 3-D multi-block-grid of the investigated bladings

from the coordinate transformation. Making use of a Newton method leads to the following approximation of the conservation equations in implicit form:

$$\frac{\Delta \mathbf{U}}{\Delta t} + (\underline{\mathbf{A}}^n \cdot \Delta \mathbf{U})_\xi + (\underline{\mathbf{B}}^n \cdot \Delta \mathbf{U})_\eta + (\underline{\mathbf{C}}^n \cdot \Delta \mathbf{U})_\zeta = -(\mathbf{E}_\xi^n + \mathbf{F}_\eta^n + \mathbf{G}_\zeta^n) = \mathbf{RHS} \quad (5)$$

where  $\underline{\mathbf{A}}, \underline{\mathbf{B}}, \underline{\mathbf{C}}$  are the Jacobians of the fluxes  $\mathbf{E}, \mathbf{F}$  and  $\mathbf{G}$ . The solution vector  $\mathbf{U}^{n+1}$  at the new time level can be obtained by adding  $\Delta \mathbf{U}$  to the old solution  $\mathbf{U}^n$ .

For the inviscid fluxes an upwind discretization is used. A locally one-dimensional Riemann problem is solved on each cell face. So, the transport of information is modeled in a physically correct manner. This complex calculation preserves high accuracy even with transonic flows. With respect to numerical diffusion a Godunov type flux-differencing is employed (Schmatz, 1988). In order to achieve a third order accuracy van Leer's MUSCL-technique is used (Anderson et al, 1985). Since the Godunov flux is not sufficiently diffusive to guarantee stability in regions with complex flow phenomena, it is combined with a modified Steger-Warming flux (flux vector splitting) (Eberle et al, 1985).

The viscous fluxes are approximated using central differences. The resulting system of linear equations is solved by a Gauss-Seidel point iteration scheme. The closure of the conservation equations is provided by the algebraic eddy-viscosity turbulence model by Baldwin and Lomax (1987).

Figure 2 gives an impression of the numerical grids. In order to achieve a sufficient solution of the grid and therefore to resolve

the boundary layer of the blade flow, an O-block has been applied around the blade surface, so that the first cell center in the flow region has a dimensionless wall distance of  $y^+ \leq 3.0$  around the blade. For the main flow section several H-blocks are used. In the radial direction 45 cell layers are established. For this investigation the shroud cavities have completely been neglected. The full size of the 3-D grid is about 1.3 million grid points. The boundary conditions have been derived from experimental data and are prescribed as radial distribution of the total pressure, the temperature and the flow angles  $\alpha$  and  $\beta$  at the inlet and the static pressure at the outlet. Mixing planes are applied between the vane and the blade using a flux coupling method.

## RESULTS

### a) Stage Flow Phenomena

Figure 3 a) and b) show the distribution of the relative mass flow rate for the investigated bladings at both operating points to illustrate the effects of the different blade designs. Due to the design of blading A the secondary flows near the endwall of the blading could be reduced, leading to a nearly constant mass flow

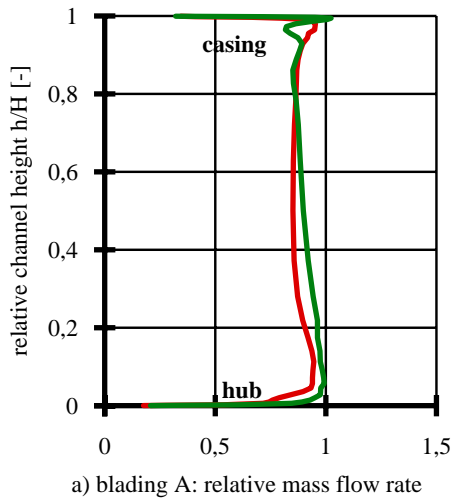
from the hub to the casing for this turbine profile.

At blading B the displacement of the flow from  $h/H=0.85$  at the tip and  $h/H=0.2$  at the hub to the middle of the flow channel can clearly be detected. The maximum mass flow at blading B can be found at  $h/H=0.3$ .

At the off-design point the blade load is increased due to a reduced rotor speed and the mass flow rate through the turbine increases slightly in the region from about 15% to 60% channel height for both bladings.

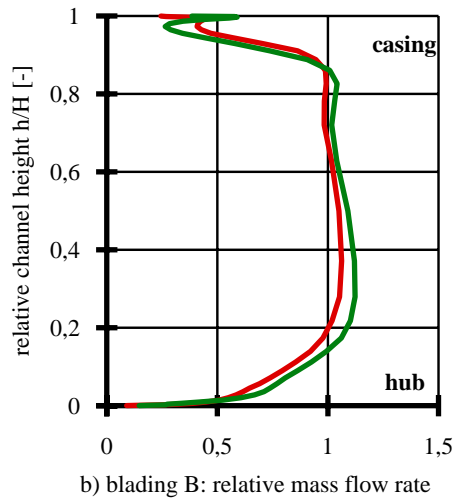
Figure 4 a) and b) show the comparison of the radial distribution of the circumferentially mass-averaged polytropic efficiency between the investigated bladings. The mass-averaged polytropic efficiency of the blading A is taken as a basis for the relative values.

At blading A the maximum polytropic efficiency is nearly constant due to the design of the blading from  $h/H=0.2$  to  $h/H=0.8$  for both operating points, analogously to the distribution of the mass flow rate. The local minima at the hub and the tip indicate the center of the channel vortices at  $h/H=0.1$  for the hub side vortex and  $h/H=0.95$  for the vortex at the casing. The relative



a) blading A: relative mass flow rate

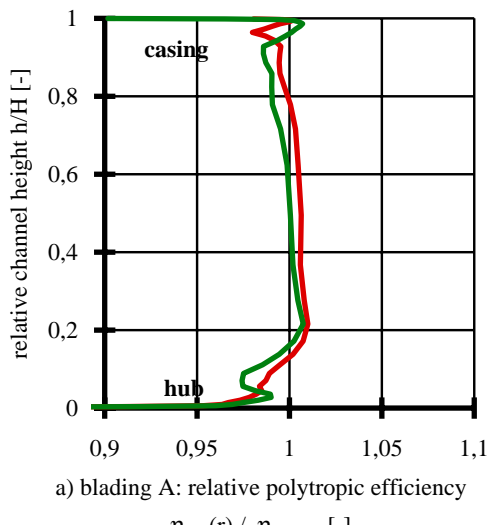
$\rho(r) \cdot u_{ax}(r) / (\rho \cdot u)_{ref} [-]$



b) blading B: relative mass flow rate

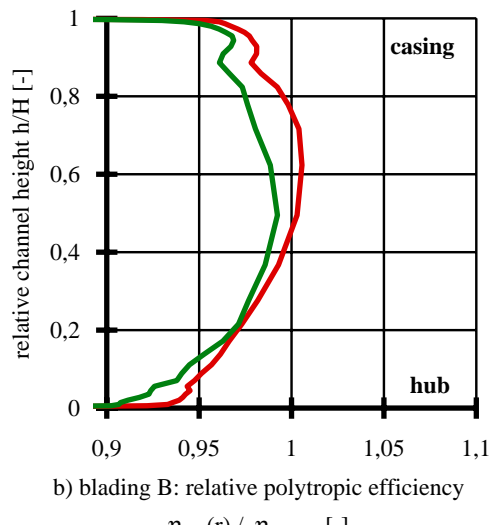
$\rho(r) \cdot u_{ax}(r) / (\rho \cdot u)_{ref} [-]$

Fig. 3 Relative mass flow rate behind the second rotor (MP 22)



a) blading A: relative polytropic efficiency

$\eta_{pol}(r) / \eta_{pol,ref} [-]$



b) blading B: relative polytropic efficiency

$\eta_{pol}(r) / \eta_{pol,ref} [-]$

Fig. 4 Radial relative polytropic efficiency of the turbines

positions of the local maxima and minima are the same for both operating points.

For the second investigated blading B the maximum polytropic efficiency can be found at  $h/H=0.6$ . From this maximum a significant decrease in efficiency both towards the hub and the casing can be determined. At the casing a local minimum, indicating the center of the passage vortex, can be found at  $h/H=0.9$ .

The increase of the blade load from OP1 to OP2 leads to a reduction of the overall efficiency of 1% for blading A and 3% for blading B. This indicates, that the blading A has a better part-load behavior compared to blading B.

### b) Secondary Flow Development

The development of the horseshoe and passage vortex of the investigated blade designs are shown in Figure 5 and 6 by means of vector plots at different cutting plane positions. The cutting planes are normal to the suction side of the blade, the scale of the vectors is the same in all planes.

The cutting planes in figure 5 show the development of the horseshoe- and the passage-vortex at the second stator vane of blading A. At  $\Delta x/X=0.1$  the horseshoe-vortex can clearly be

determined with an influence on the main flow till  $h/H=0.975$ . The center of the horseshoe vortex is at about  $h/H=0.98$ . At  $\Delta x/X=0.3$  the horseshoe-vortex is significantly influenced by the endwall flow. The formation of the passage vortex starts at about  $\Delta x/X=0.5$ . Figure 5.4 shows the developed passage vortex. The extension of the passage vortex is limited to  $h/H=0.9$  with its center at about  $h/H=0.975$ . The reduced extension of the secondary flows leads to reduced losses near the casing, corresponding to the high polytropic efficiency for the first blading till  $h/H=0.9$

The development of the secondary flow phenomena of the second investigated blading B is shown in figure 6. Analogously to blading A the horseshoe-vortex can clearly be determined at  $\Delta x/S=0.1$ . In contrast to the first blading the influence on the main flow is enhanced significantly. Also analogously to the first blading at  $\Delta x/X=0.3$  the influence of the passage flow on the horseshoe-vortex can be determined. The formation of the passage vortex of the second blading can be seen in figure 6.3 at about  $\Delta x/S=0.5$ . The developed passage vortex can be seen in figure 6.4. In contrast to blading A the intensity of the passage vortex is reduced, but the extension is significantly enhanced. The center of the passage vortex is at about  $h/H=0.9$ . Due to the enlarged

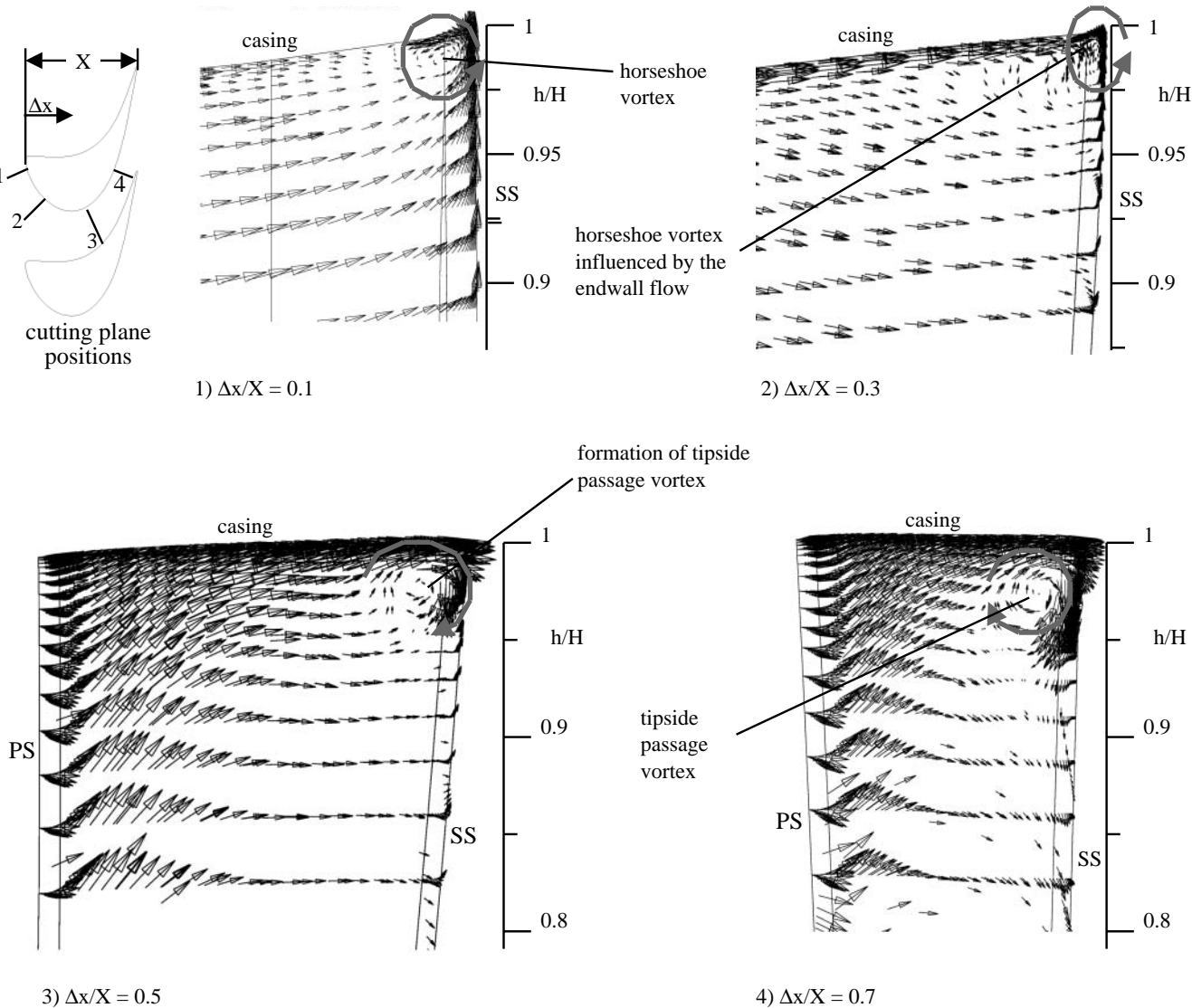


Fig. 5 Secondary flow development, blading A, 2nd stator vane

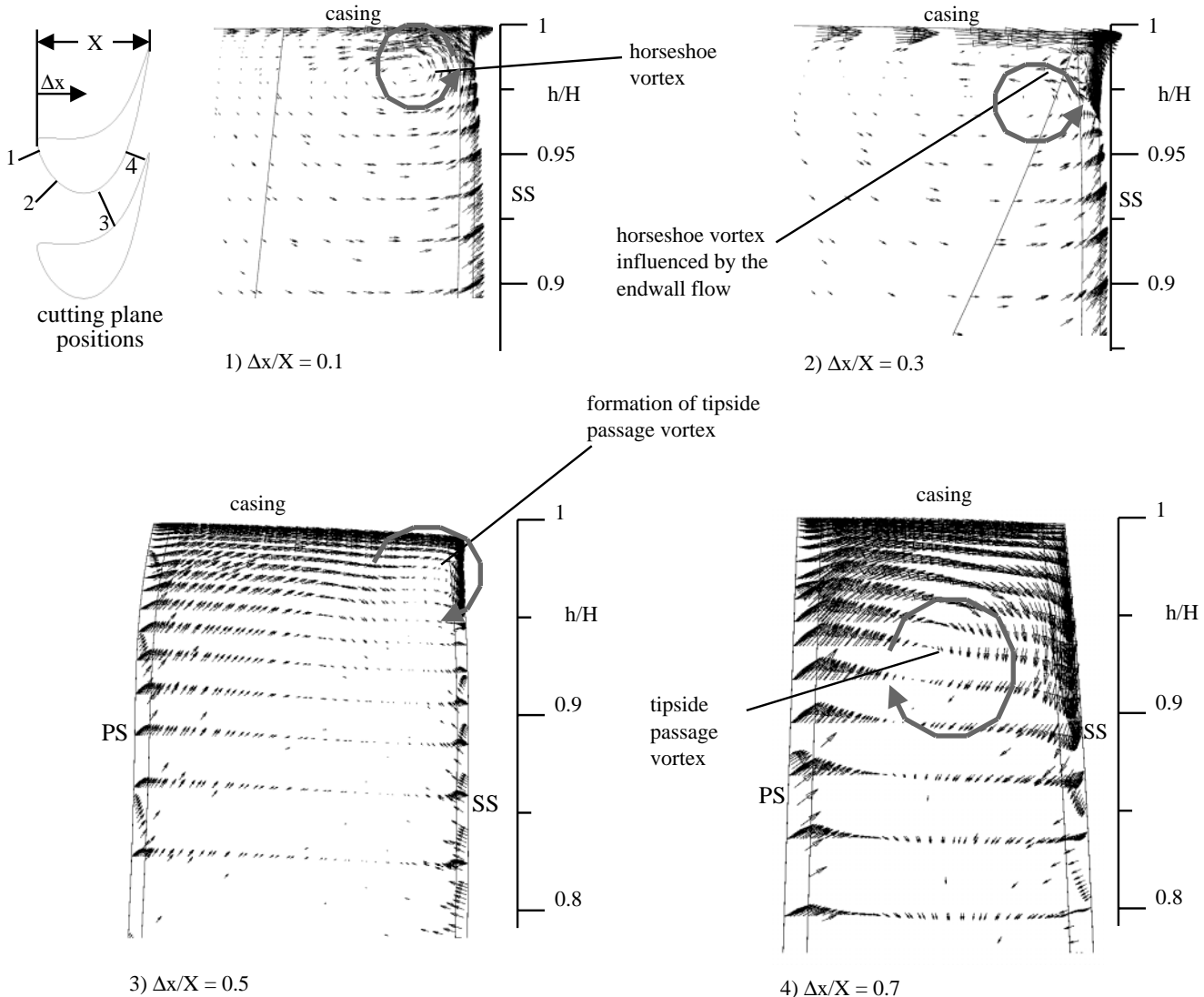


Fig. 6 Secondary flow development, blading B, 2nd stator vane

secondary flow region of blading B the significant drop of the polytropic efficiency can be explained.

### c) Comparison to Experimental Data

A comparison of the numerical results and experimental data for the investigated bladings is shown in figure 7 and figure 8. The circumferentially averaged numerical values of the flow angles and the total pressure are compared to steady probe measurements for the blading A in figure 7 and blading B in figure 8 at the measuring plane MP22 at operating point OP1.

At blading A the distribution of the swirl angle  $\alpha$  shows the center of the passage vortex at the casing at  $h/H=0.9$  to  $0.95$  both for the experimental and the numerical investigation. A difference between the numerical and the experimental results occurs at the hub, where the hub side passage vortex is predicted less compared to the experimental results. The high measured pitch angle  $\beta$  at the tip results from an interaction of the probe with the endwall flow.

Looking at the swirl angle  $\alpha$  at blading B, the influence of the tipside passage vortex can be detected till  $h/H=0.8$  both for the numerical and experimental results. Analogously to blading A the numerical and experimental results differ mainly at the hub side of the blading.

Although the basic flow phenomena are reasonably captured

and the levels of the values are in good agreement, some differences occur due to the neglected shroud cavities and their influence on the flow, in spite of the small gap size between the cavity and the main flow. To determine the influence of the cavities, numerical and experimental investigations have been pursued (Bohn et al. 2003). Further differences occur due to multi-stage interaction which cannot be taken into account in the numerical simulations with a steady code. Nevertheless, the numerical results help to understand origin and development of the main flow phenomena as shown below.

### CONCLUSIONS

This paper presents a numerical investigation of the flow field in a 2-stage axial turbine with shrouded-rotor cavities for two different blade designs. Blading A is designed to achieve a radially homogenous flow through the passage by decreasing the secondary flow regions at the endwall of the blades. In contrast blading B concentrates the main flow to the middle of the passage. Using one of the turbine test rigs at the Institute of Steam and Gas Turbines, Aachen University, experimental results were also obtained for both bladings. For this study the experimental results have been used as boundary conditions for the numerical multi-stage calculations of the 3D flow through the 2-stage turbine.

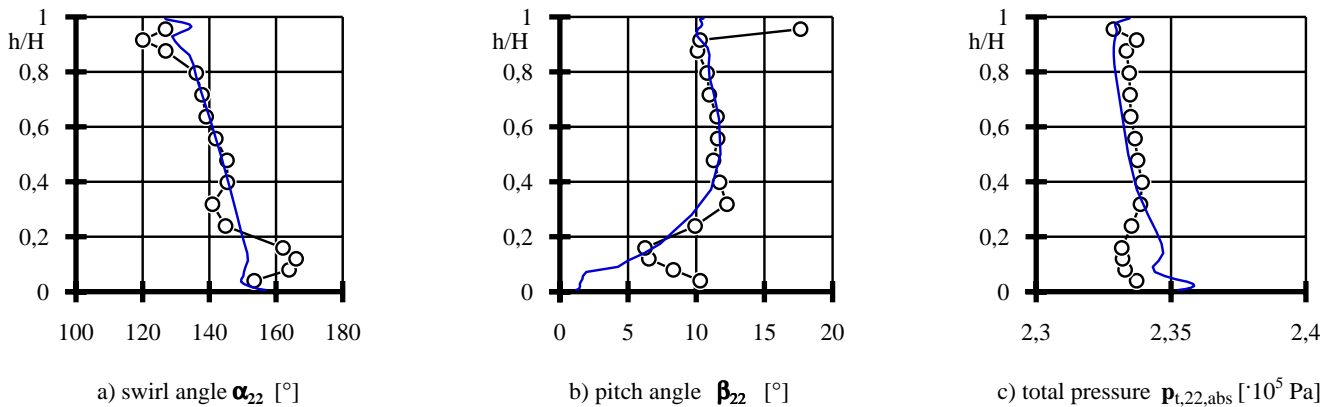


Fig. 7 Comparison of numerical results with experimental data behind 2nd stage (MP22), blading A,  
OP1 (o—o experiment — numerical simulation)

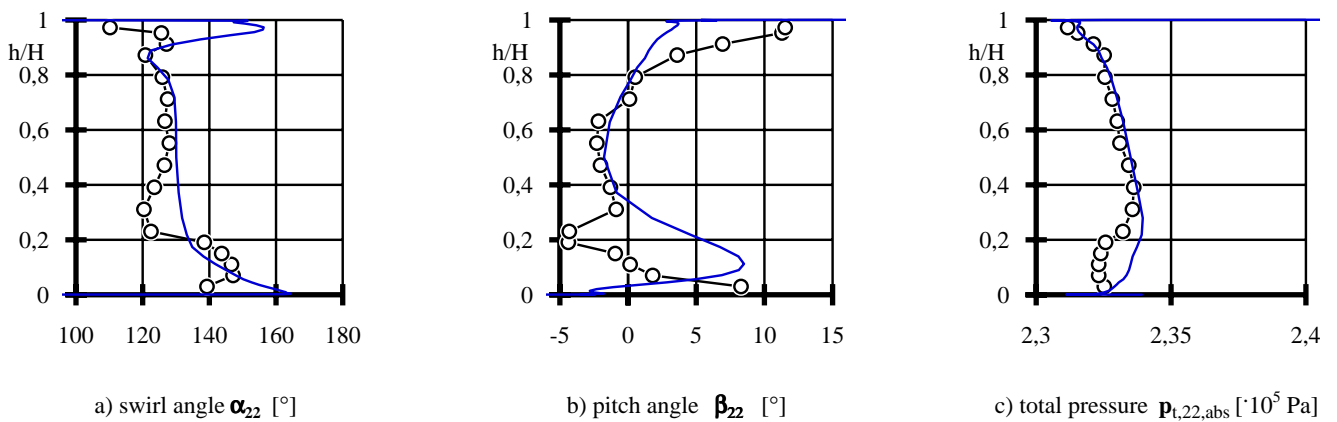


Fig. 8 Comparison of numerical results with experimental data behind 2nd stage (MP22), blading B,  
OP1 (o—o experiment — numerical simulation)

The numerical results show the following:

1. Due to a reduction of the extension of the secondary flows near the hub and the casing a radial homogeneous mass flow through the channel can be achieved for blading A.
2. The radial homogenous mass flow through the channel at blading A results in a radially homogenized distribution of the polytropic efficiency for the turbine.
3. The concentration of the mass flow to the middle of the blade passage at blading B will lead to significantly enlarged secondary flow losses near the hub and the casing.
4. Due to the enlarged secondary flow phenomena a drop of efficiency occurs in the endwall regions for blading B.

#### ACKNOWLEDGEMENTS

The investigations were performed as a part of the joint research program "500 MW auf einer Welle (AG Turbo II)". The work was supported by the Bundesministerium für Wirtschaft (BMWI) under file number 0327061E. The authors gratefully acknowledge AG Turbo and ALSTOM Power for their support and permission to publish this paper. The responsibility for the content lies with the authors.

#### RERERENCES

- Anderson, W. K., Thomas, J. L., van Leer, B. A., 1985, "Comparison of Finite Volume Flux Vector Splittings for the Euler Equations", *AIAA-paper 85-0122*
- Baldwin, B. S., and Lomax, H., 1978, "Thin Layer Approximation and Algebraic Model for Separated Turbulent Flows", *AIAA-paper 78-257*
- Bassi, F., Savini, M., 1992, "Secondary Flows in a Transonic Cascade: Validation of a 3-D Navier-Stokes Code", *ASME paper 92-GT-62*
- Bohn, D., Sürken, N., Yu, Q., Kreitmeier, F., 2002, "Axisymmetric Endwall Contouring in a Four-Stage Turbine - Comparison of Experimental and Numerical Results", *ASME Paper GT2002-30351*
- Bohn, D., Gier, J., Emunds, R., Jennions, I.K., 1997, "The Computation of Adjacent Blade-Row Effects in a 1.5 Stage Axial Flow Turbine", *ASME Paper 97-GT-81*
- Bohn, D., Rudzinski, B., Sürken, N., Gärtner, W., 2000, "Experimental and Numerical Investigation on the Influence of Rotorblades on Hot Gas Ingestion into the Upstream Cavity of an Axial Turbine Stage", *ASME Paper ASME2000-GT-284*
- Bohn, D. E., Balkowski, I., Ma, H., Tümmers, C., Sell, M., 2003, "Influence of Open and Closed Shroud Cavities on the Flowfield in a 2-Stage Turbine with Shrouded Bladings", *ASME GT2003-38436, ASME Turbo Expo 2003, Atlanta, USA*

Eberle, A., Schmatz, M. A., Bissinger, N., 1990,  
"Generalized Flux Vectors for Hypersonic Shock-Capturing",  
*AIAA -paper 90-0390*

Hirsch, Ch., 1994, "CFD Methodology and Validation for Turbomachinery Flows", *AGARD Lectures Series 'Turbomachinery Design Using CFD'*

Marchal, P. , Sievering, C. H., 1977, "Secondary Flows Within Turbomachinery Bladings", *AGARD CP 214*

Moore, J., Smith, B. L., 1983, "Flow in a Turbine Cascade. Part 2: Measurement of Flow Trajectories by Ethylene Detection", *ASME 83-GT-69*

Nikolaou, I.G., Papailiou, K.D., Giannakoglu, K.C., 1997, "Numerical Prediction of the Secondary Flow in A Turbine Cascade", *ISABE 97-7103*

Schmatz, M.A., 1988, "Three-dimensional Viscous Flow Simulations Using an Implicit Relaxation Scheme", *Notes on Numerical Fluid-Mechanics (NNFM)*, 22, Vieweg, Braunschweig, pp. 226-242

Sieverding, C. H., 1984, "Recent Progress in the Understanding of Basic Aspects of Secondary Flow in Turbine Blade Passages", *ASME 84-GT-78*

Sieverding, C. H., Van den Bosch, P., 1983, "The Use of Coloured Smoke to Visualize Secondary Flows in a Turbine-Blade Cascade", *Journal of Fluid Mechanics*, Vol. 134

Van den Braembussche, R. A., Sieverding, C. H., Maretto, L. A., Sabattini, A., 2001, "Turbine Stage Optimization by means of a full 3D blade design concept", *4th European Conference on Turbomachinery Fluid Dynamics and Thermophysics, Firenze, Italy*

Zimmermann, H., 1992, "Calculation of Three-Dimensional Transonic Turbine Cascade Flow", *Journal of Propulsion und Power*, Vol. 8, No. 2